similar diameter (that is, samples 2 and 1, respectively). We believe that this comparison demonstrates the importance of studying individual nanotubes that are structurally characterized to determine their intrinsic properties. It is also interesting to consider if it will be possible, by introducing defects directly with the probe tip or by other means, to probe systematically the effects of electron scattering in these one-dimensional structures.

The sensitivity of resistivity to structural imperfections must be accounted for to determine ultimately the intrinsic conductivity of nanotubes but may also allow tailoring of the resistance of these materials for applications. We believe that our experimental approach opens the door to developing a clear understanding of nanotube electrical transport and to testing theoretical predictions, although this will require careful studies of the temperature and diameter dependencies of the resistivity in structurally characterized samples. The approach outlined here should be applicable to probing of the intrinsic electrical properties of metal-filled nanotubes (*18*), carbide nanorods (*11*), and boron nitride nanotubes (*19*) and furthermore may be able to assess the validity of the term "molecular wire," which has been widely applied to organic and biological nanostructures (*1*, *7*). Lastly, we note that the experimental approach outlined in Fig. 1 can be generalized to measure the mechanical properties of nanomaterials and thereby address their applicability in composites and other structural systems (*20*).

REFERENCES AND NOTES

1. C. A. Mirkin and M. A. Ratner, *Annu. Rev. Phys. Chem.* **43**, 719 (1992); J.-M. Lehn, *Angew. Chem. Int. Ed. Engl.* **29**, 1304 (1990); C. F. van Nostrum, S. J. Picken, A.-J. Schouten, R. J. M. Nolte, *J. Am. Chem. Soc.* **117**, 9957 (1995).
2. C.-G. Wu and T. Bein, *Science* **266**, 1013 (1994).
3. T. W. Ebbesen, *Annu. Rev. Mater. Sci.* **24**, 235 (1994).
4. S. Iijima, *Nature* **354**, 56 (1991).
5. T. W. Ebbesen and P. M. Ajayan, *ibid.* **358**, 220 (1992).
6. M. S. Dresselhaus, *ibid.*, p. 195; J. W. Mintmire, B. I. Dunlap, C. T. White, *Phys. Rev. Lett.* **68**, 631 (1992); N. Hamada, S. Sawada, A. Oshiyama, *ibid.*, p. 1579; R. Saito, M. Fujita, G. Dresselhaus, M. S. Dresselhaus, *Appl. Phys. Lett.* **60**, 2204 (1992); G. Overney, W. Zhong, D. Tomanek, *Z. Phys. D* **27**, 93 (1993).
7. C. J. Murphy *et al.*, *Science* **262**, 1025 (1993); T. J. Meade and J. F. Kayyem, *Angew. Chem. Int. Ed. Engl.* **34**, 352 (1995).
8. W. A. de Heer *et al.*, *Science* **268**, 845 (1995).
9. L. Langer *et al.*, *J. Mater. Res.* **9**, 927 (1994).
10. G. M. Whitesides and C. S. Weisbecker, *Mater. Res. Soc. Symp. Proc.* **349**, 263 (1994).
11. H. Dai, E. W. Wong, Y. Z. Lu, S. Fan, C. M. Lieber, *Nature* **375**, 769 (1995).
12. C. E. Snyder *et al.*, International Patent WO 89/07163 (1989).
13. The straight, catalytically grown nanotubes may have a higher defect density than arc-grown samples, although we believe that their overall structures are quite similar. The central objective of this work is to demonstrate an approach that can measure conductivity and structure simultaneously in nanomaterials.
14. R. Hoper *et al.*, *Surf. Sci.* **311**, L731 (1994).
15. D. L. Wilson, K. S. Kump, S. J. Eppell, R. E. Marchant, *Langmuir* **11**, 265 (1995); C. Odin, J. P. Aime, A. El Kaakour, T. Bouhacina, *Surf. Sci.* **317**, 321 (1994); J. E. Griffith and D. A. Grigg, *J. Appl. Phys.* **74**, R83 (1993).
16. The experimentally derived expression relating the annular cross-sectional area to measured OD is $A_{cross} = a + bx + cx^2$, where x is the OD in angstroms, $a = (-2.67 \pm 0.91) \times 10^{-17}$ m^2, $b = (4.73 \pm 1.6) \times 10^{-19}$ m^2/Å, and $c = (4.72 \pm 0.69) \times 10^{-21}$ m^2/Å^2.
17. Defects in multishell nanotubes increase the resistivity through electron scattering relative to an ideal structure. The lowest values we observed were still nearly a factor of 20 greater than that observed for crystalline graphite and may be an indication of scattering by such extrinsic defects. Because inner shells of multishell nanotubes cannot be probed directly by force microscopy, we believe that studies of single-shell nanotubes (*3*) ultimately provide the best measure of the intrinsic conductivity of nanotubes. It would also be possible to compare measurements of single-shell nanotubes directly with theory (*4*), whereas multishell nanotubes have not been investigated in detail theoretically.
18. P. M. Ajayan and S. Iijima, *Nature* **361**, 333 (1993); S. C. Tsang, Y. K. Chen, P. J. F. Harris, M. L. H. Green, *ibid.* **372**, 159 (1994); C. Guerret-Piecourt, Y. Le Bouar, A. Loiseau, H. Pascard, *ibid.*, p. 761.
19. N. G. Chopra *et al.*, *Science* **269**, 966 (1995); O. Stephan *et al.*, *ibid.* **266**, 1683 (1994).
20. Mechanical properties of nanotubes and nanorods, such as elastic modulus and fracture strength, can be probed by using the lateral force sensing capabilities of the microscope to measure force versus displacement curves (E. W. Wong, P. E. Sheehan, C. M. Lieber, unpublished results).

21. We thank J. Liu and J. Huang for help in the design and fabrication of the electronics used in these measurements. C.M.L. acknowledges partial support of this work by the Materials Research Science and Engineering Center of the National Science Foundation under award DMR-9400396 and by the Office of Naval Research.

20 December 1995; accepted 22 February 1996

Teleconnections Between the Subtropical Monsoons and High-Latitude Climates During the Last Deglaciation

F. Sirocko,* D. Garbe-Schönberg, A. McIntyre, B. Molfino

The major deglacial intensification of the southwest monsoon occurred at 11,450 ± 150 calendar years before present, synchronous with a major climate transition as recorded in Greenland ice. An earlier event of monsoon intensification at 16,000 ± 150 calendar years before present occurred at the end of Heinrich layer 1 in the Atlantic and parallels the initial rise in global atmospheric methane concentrations and the first abrupt climate changes in the Antarctic; thus, the evolution of the monsoonal and high-latitude climates show teleconnections but hemispheric asymmetries. Superimposed on abrupt events, the monsoonal climate shows high-frequency variability of 1785-, 1450-, and 1150-year oscillations, and abrupt climate change seems to occur when at least two of these oscillations are in phase.

Major regions of the Northern Hemisphere are influenced either by Atlantic-controlled winds and precipitation or by the monsoons (Fig. 1). To evaluate physical links between these two large-scale systems, we compared their climatic history during the transition from the last glacial epoch into the Holocene as recorded in Greenland ice cores and in deep-sea sediments from the Arabian Sea. First observed by Dansgaard *et al.* (*1*) and confirmed by the ice cores of the Greenland Ice Core Project (GRIP) and Greenland Ice Sheet Project II (GISP2) (*2*, *3*), the first abrupt deglacial warming event over the North Atlantic and Greenland occurred 14,500 ± 150 calendar years before present (B.P.), followed by another warming event at 11,600 ± 150 calendar years B.P. (Fig. 2). The increase in global atmospheric methane concentrations, in contrast, as recorded in the GRIP ice core, started about 16,000 calendar years B.P. (*4*), indicating an early onset of environmental change in the tropics, where most of the modern methane is produced in wetlands. The first deglacial change in wind trajectories and dust content over Antarctica also started at about 16,000 calendar years B.P. (*5*), that is, also significantly earlier than the first temperature increase in Greenland (Fig. 2). Accordingly, the climate of the high latitudes in the Northern and Southern hemispheres show strong regional contrasts.

To compare this asymmetric evolution of the polar climates with the evolution of the subtropical monsoons, we used data (*6*) from core 74KL from the upwelling area of the western Arabian Sea (Fig. 1), where five abrupt $\delta^{18}O$ changes have been ob-

F. Sirocko and D. Garbe-Schönberg, Geological-Paleontological Institute, University Kiel, Olshausenstrasse 40-60, 24118 Kiel, Germany.
A. McIntyre and B. Molfino, Lamont-Doherty Earth Observatory, Palisades, NY 10964, USA.

*To whom correspondence should be addressed at Geoforschungszentrum Potsdam, Am Telegrafenberg A17, 14473 Potsdam, Germany.

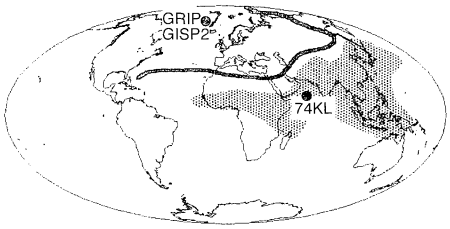

Fig. 1. Areas affected by monsoon precipitation (gray region) (equal area projection, modified from IGCP-349 planning report) and by precipitation derived from the Atlantic-European westwind drift (eastern extent marked by heavy curve). Drilling locations of the Greenland ice-core projects (GRIP and GISP2) and sediment core 74KL are shown for reference.

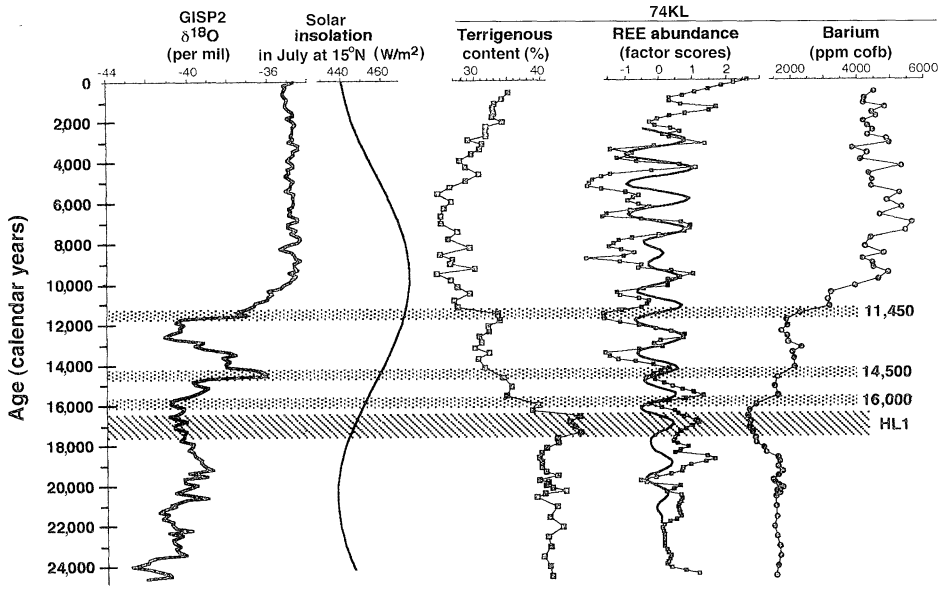

Fig. 2. Age correlation between abrupt climatic changes in Greenland (GISP2 ice core) and those in the monsoon region (74KL). Methods and units are described in (*6, 26*). The $\delta^{18}O$ data and age model for GISP2 are from (*3, 34, 39*). The $\delta^{18}O$ data were resampled at 150-year intervals and represent the input data for the cross-spectral analysis (Fig. 4). Stippled bars indicate times of abrupt events in monsoonal climate in U/Th-adjusted ^{14}C years (*7*). The age of HL1 is from (*13*). The continuous line without markers in the REE plot shows the amplitude variations in Fig. 5. The U/Th adjustment of the ^{14}C dates for core 74KL follows the procedure of Bard *et al.* (*14*) and is documented in (*7*). Bard *et al.* (*40*) recently showed their older (*14*) U/Th adjustment scheme to produce ages 500 years too old for glacial ages >18,000 calendar years B.P. To keep the stratigraphy of this paper consistent with our older papers (*7, 11*), we have used the ages as published in (*7*).

served and dated by an accelerator mass spectrometry (AMS) ^{14}C chronology (*7*); the major $\delta^{18}O$ events are centered at 16,000, 11,450, and 9900 calendar years B.P. Our proxy indicator for aridity and humidity in Arabia is the abundance of terrigenous matter (*6*), which is largely eolian, being today derived from Arabian desert dust settling from mid-tropospheric northwesterly winds during summer (*8*), with some minor contributions from East Africa and the Persian Gulf region (*9, 10*). During glacial times, much larger proportions of dust were also derived from the Persian Gulf area and northern India (*10, 11*). Proxy indicators of southwest monsoon strength are cadmium (Cd) and barium (Ba) content, which reflect the flux of organic matter from the southwest-monsoon–driven upwelling in the western sector of the Arabian Sea (*11, 12*). The variations of these tracers in core 74KL record 18,000 to 16,500 calendar years B.P. as a late glacial minimum in the intensity of southwest-monsoon–driven upwelling productivity, paralleled by maximum dust flux, and thus, maximum aridity in Arabia (Fig. 2).

This interval of low southwest-monsoon intensity coincides with Heinrich layer 1 (HL1), the time of massive iceberg discharge from the Laurentide Ice Sheet into the western and central Atlantic, dated at 14,800 to 13,500 ^{14}C years ago (*13*) [corresponding roughly to 18,300 to 17,000 calendar years B.P. (*14*)]. Major iceberg surges in the Norwegian Sea originated from the Barents Shelf 14,200 to 13,200 ^{14}C years B.P. (17,700 to 16,700 calendar years B.P.) (*15*), just within HL1. Accordingly, the initial decay of the Fennoscandian Ice Sheet occurred at the same time or slightly after the breakup of the Laurentide Ice Sheet. A close connection between the Atlantic Heinrich layers and the Asian winter monsoon has already been documented by strong loess transport in central China during times of all Heinrich layers (*16*); our data show that these teleconnections also existed in the summer season. Unresolved is the question of whether the connection is mediated by the intensity of Asian winter, winter to summer snow depth (*17*), or a true teleconnection during the summer season.

The rapid reduction of terrigenous matter in core 74KL at 16,000 calendar years B.P., near the end of HL1, should reflect a reduction of dust flux from Arabia paralleling a general increase of humidity on the peninsula. The same transition was reflected in East African lake levels (*18*), global atmospheric methane levels (Fig. 2), and an increase in temperature and decrease in dust content over Antarctica (*5*). Apparently, the Southern Hemispheric polar climate had a tight connection to the climate of the subtropics during this early event of monsoon intensification, at a time when Greenland was still under full glacial conditions.

The next event in the monsoonal climate, at 14,500 calendar years B.P., was not clearly visible in the *Globigerinoides ruber* $\delta^{18}O$ record of 74KL (*7*) but is poorly yet significantly defined in the upwelling (Ba) and dust flux (terrigenous) record (Fig. 2). This event was the most pronounced change in climate over Greenland, the Bølling transition (*3*), but was not observed over Antarctica (*5*). The Allerød and Bølling interval reveals a southwest-monsoon intensity well below that during the Holocene. The Younger Dryas is barely observable in the record of upwelling (Ba) but is associated with an increase of terrigenous matter, mainly of those proportions that were also abundant during glacial times, derived from the Persian Gulf area or transported from Pakistan and India by strong northeast-monsoon winds (*11, 19*). Later, at the end of the Younger Dryas, the intensity of the summer southwest monsoon increased greatly at 11,450 ± 150 calendar years B.P. (Ba, Fig. 2), paralleled by a sharp reduction of dust flux, mainly of those proportions derived from the north (*11*). This climate transition during both winter and summer appears to coincide with the major climatic amelioration in the North Atlantic region and Europe (*20*) dated at 11,650 ± 150 calendar years B.P. in the Greenland ice cores (Fig. 2). This change is, however, barely visible in the Antarctic temperature record (*5*). A subsequent increase in monsoon intensification at 9700 calendar years B.P. has no clear corresponding pattern in the North Atlantic nor in the Antarctic climate (Fig. 2). The Greenland temperature increase reached its Holocene level at this time, but temperatures over Antarctica were already beginning to decrease.

Discussion about the possible forcing mechanisms of abrupt climate change on time scales of decades and centuries has

highlighted three mechanisms that are regarded as having the greatest potential to affect climate on a global scale (*21*): (i) fresh water fluxes into the North Atlantic effecting the northward flow of heat-exporting ocean surface currents and the thermohaline-driven conveyor belt of the deep-ocean circulation, (ii) internal oscillations in the stability of the Laurentide Ice Sheet, with effects on scenario (i), ice sheet topography, and atmospheric wind trajectories, and (iii) variations in the atmosphere's water-vapor content, the most effective greenhouse gas.

The observation that not all abrupt climate changes are synchronous between Antarctica and Greenland but that the subtropical monsoon climate shares features with the climatic evolution in both polar hemispheres suggests that the cause of large-scale climatic changes might lie in the low latitudes, possibly mediated to the high latitudes by means of water vapor export. In contrast to atmospheric CO_2 and methane, which have long residence times in the atmosphere and are mixed to globally similar concentrations within a few years, water vapor is regarded as having the largest potential to cause hemispherically asymmetric heating effects (*22*).

The synchroneity and geographical extent of events alone do not allow us to draw any conclusive inference on the physical cause of events. Thus, we explored if the events in the monsoonal record also have an oscillatory nature, similar to the 2000- to 3000-year Dansgaard-Oeschger cycles of the North Atlantic and Greenland climate (*23*).

The geochemical upwelling records of Ba (Fig. 2) and Cd (*11*) and the *Globigerina bulloides* abundance (*24*), a faunal upwelling indicator (*25*), reveal periodicities of 1785 and ~1150 years in core 74KL (Fig. 3, A and B). The abundance of terrigenous matter, specifically dolomite [a tracer of dust from the Persian Gulf area (*10*)] and Mg content, which reflects changes in dolomite- and palygorskite-rich summer dust discharge by northwesterlies from north Arabia, show a period near 1450 years (Fig. 3, D and E), which is still more pronounced, and visually apparent, in the abundance of the rare earth elements (REEs) when spectra are prewhitened (Fig. 3F) (*26*). A 2800-year period is also embedded in the variations of REE content, almost blanketed in the prewhitened spectra of Fig. 3, but dominating in the unprewhitened cross-spectra of Fig. 4. The highest significant period in the 74KL record is near 1000 years, for example, in the REE record or rubidium (Rb) to aluminum (Al) ratio (Figs. 3 and 5).

Pestiaux *et al.* (*27*) reported suborbital periodicities at 4600 and 2300 years in the

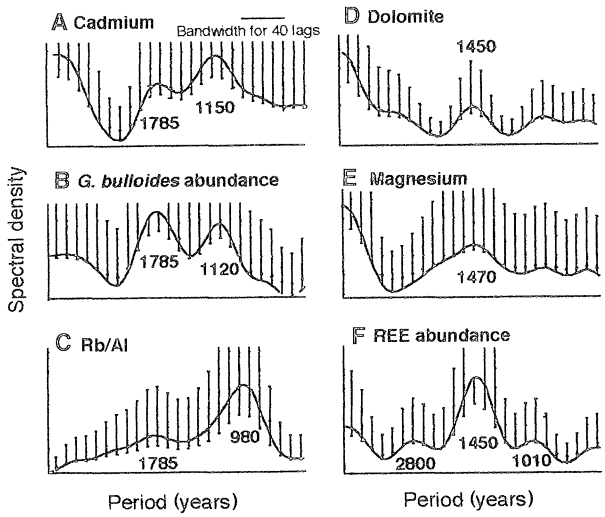

Fig. 3. Prewhitened spectra (0.8 level) of geochemical tracers in sediment core 74KL. Upwelling tracers: (**A**) Cd content (southwest-monsoon–driven upwelling) and (**B**) *Globigerina bulloides* abundance. Dust discharge tracers: (**C**) Rb/Al (northeast monsoon), (**D**) dolomite content (Arabian northwesterlies), (**E**) Mg content (Arabian northwesterlies), and (**F**) REE factor 1 (Arabian northwesterlies).

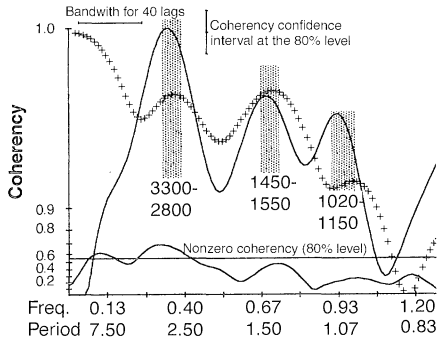

Fig. 4. Cross-spectra (lower solid trace) between REE element abundance (*26*) in core 74KL (relative variation indicated by crosses) and $\delta^{18}O$ of ice in the GISP2 ice core (*3, 34*) (relative variation indicated by upper solid trace), using the time scale of (*39*). The period is measured in thousands of calendar years, and the frequency is the inverse of the period. Sample spacing in core 74KL is 200 to 250 years, resampled at 150 years. Sample spacing in the GISP2 record is also at 150 years, but values are averaged for intervals spanning 100 years (resolution of the raw data is based on a 2-m sampling interval, translating to 5-year resolution during the Holocene, continuously decreasing to 150-year resolution during the last glacial maximum). To account for the smoothing effect of bioturbation in deep-sea core 74KL, the GISP2 $\delta^{18}O$ data were also smoothed with a 3-point average.

Indian Ocean hydrography, which were explained as combination tones of the orbital precessional and obliquity cycles, representing an internal but nonlinear response of the monsoon system to solar forcing (*28*). A similar 2200-year periodicity was reported from the Oman margin (*29*) and attributed to interactions between oceanic circulation changes and atmospheric ^{14}C variations, which show a 2300-year periodicity (*30*). Higher frequency periodicities (1610 to 1800 years, 1150 to 1280 years, and 880 to 960 years during Termination II and III), similar to those we see, were reported from paleotemperature variations in the upwelling off west Africa (*31*) and from vegetation changes in the southeastern United States (*32*) (1224-year and 1425-year periods). The 1450-year and 1150-year periods have also been found in the $\delta^{18}O$ (temperature) record of the Camp Century ice core in Greenland (*33*). Thus, all of the frequencies observed in the monsoonal climate appear to be part of global climate oscillations.

Oscillations in a high-resolution, 16,500-year $\delta^{18}O$ record from the GISP2 ice core reveal various periodicities below 1000 years and 1050-year and 3300-year periods during the periodicity range of our study (*34*). A cross-spectral analysis of the REE abundance in core 74KL and $\delta^{18}O$ of ice in the GISP2 record reveals coherency well above the 80% significance level in the 2800- to 3300-year band (Fig. 4), whereas Cd content and $\delta^{18}O$ in the ice is coherent in the 1000- to 1150-year band. Phase relations between the ice and monsoon records were not calculated because the age model of the GRIP and GISP2, which agree very well for the last 16,500 years, show inconsistencies for the time before 16,500 years B.P.

Instead, we further filtered the 74KL records at all major periodicities to obtain the variations of their amplitude (Fig. 5). The 1785-year and 1150-year periods in variations of surface water nutrient content (Cd) become fully developed only after the transition from the Younger Dryas to the Holocene at 11,450 calendar years B.P. (Fig. 5, A and B); respective filter series of the *Globigerina bulloides* abundance show the same pattern. The 1450-year period in dust flux, in contrast, was operating continuously (Figs. 4 and 5C), as was the 950-year period in Rb/Al, monitoring winter dust. All amplitude variations show a maximum

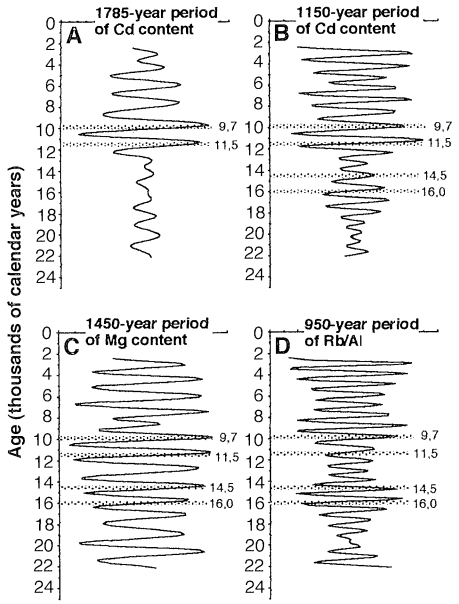

Fig. 5. Sinusoids of filtered periods; (**A**) 1785-year period in the Cd record (surface-water nutrient content), (**B**) 1150-year period in the Cd record, (**C**) 1450-year period in Mg record (dust discharge by Arabian northwesterlies), and (**D**) 950-year period in Rb/Al record (dust discharge by the northeast monsoon).

at 10,000 calendar years B.P. during the time of maximum solar insolation at subtropical northern latitudes (Fig. 2) (*35*). In particular, the envelope of the 1450-year amplitude variations for Mg (Fig. 5C) approximates a precessional oscillation. This observation and our finding that almost all sub-Milankovitch periodicities observed in Arabian Sea deep-sea cores are harmonic tones ($4600 \times 5 = 23{,}000$; $3300 \times 7 = 23{,}100$; $2300 \times 10 = 23{,}000$; $1785 \times 13 = 23{,}205$; $1450 \times 16 = 23{,}200$; and $1150 \times 20 = 23{,}000$ years) of the Earth's precessional cycle [average of 23,070 years (*36*)] suggests that these periodicities could be an internal response within the monsoon climate system to its major forcing, the precessional cycle of solar insolation strength (*12*, *37*), a mechanism having been also identified for climate variability in the 10,000- to 12,000-year band in deep-sea cores from the equatorial Pacific and Atlantic (*28*).

The amplitude of all high-frequency oscillations observed in the monsoonal climate reveal a coherent and in-phase increase toward maximum values during all major abrupt events of monsoon intensification (16,000, 14,500, 11,450, and 9700 calendar years B.P.) (Fig. 5). We cannot definitively conclude from our data whether this relation between events and oscillations is just a coincidence or if there is an underlying physical cause-effect relation. The hemispheric asymmetry of the teleconnections during abrupt events, as well as the occurrence of the same periodicities in various regions, suggests a possible relation between past abrupt climate change and internal oscillations in the global climate system, a mechanism likely to be enforced by the precessional cycle of variations in solar insolation strength at low latitudes.

REFERENCES AND NOTES

1. W. Dansgaard, S. J. Johnsen, H. B. Clausen, C. C. Langway Jr., in *Late Cenozoic Ice Ages*, K. Turekian, Ed. (Yale Univ. Press, New Haven, CT, 1970), pp. 37–56.
2. S. J. Johnsen *et al.*, *Nature* **359**, 311 (1992).
3. P. M. Grootes, M. Stuiver, J. W. C. White, S. Johnsen, J. Jouzel, *ibid.* **366**, 552 (1993).
4. J. Chappellaz *et al.*, *ibid.*, p. 443.
5. J. Jouzel *et al.*, *Clim. Dyn.* **11**, 151 (1995).
6. Terrigenous matter content in core 74KL was calculated by subtracting $CaCO_3$ content, biogenic-opal content, and organic C content from the bulk, numerical values in (*11*). For the geochemical analyses, 250 mg of each bulk sample in a Teflon beaker was moistened with 1 ml of H_2O and 2 ml of HNO_3 (10 M). The sample was heated for 2 hours at 100°C and dried to dissolve carbonate and attack organics. Then 4 ml of HF (20 M) and 1 ml of HNO_3 (10 M) were added, and the mixture was heated for 24 hours in closed vials at 160°C. The solution was dried and 1 ml of HNO_3 and 10 drops of $HClO_4$ (16 M) were added to the residue, which was then heated for 24 hours at 160°C and dried at 220°C. The residue was dissolved in 2 ml of HNO_3, and this solution was made up to a volume of 50 ml with deionized water. All analyses were done at the Geological-Paleontological Institut, University of Kiel. For full documentation, see (*11*). The Rb and REEs were analyzed on a VG PlasmaQuad PQ 1 inductively coupled plasma mass spectrometer (ICP-MS) (*38*). The Cd was measured on a Perkin-Elmer Zeeman 5000 electrothermal atomic absorption spectrometer from the same solution as the ICP-MS samples. We added 20 ml of a matrix modifier (mixture of equal parts of $PdNO_3$, $MgNO_3$, and HNO_3) to 1000 ml of the solution. Both Al and Mg were measured on a Perkin-Elmer ICP/6000. All concentrations were measured from a solution of the bulk sample, but values are expressed on a carbonate- and opal-free basis (c of b).
7. F. Sirocko *et al.*, *Nature* **364**, 322 (1993).
8. F. Sirocko and M. Sarnthein, in *Paleoclimatology and Paleometeorology: Modern and Past Patterns of Glacial Atmospheric Transport*, M. Leinen and M. Sarnthein, Eds. (NATO Advanced Study Institutes Series C, Kluwer Academic, Dordrecht, 1989), vol. 282, pp. 401–433.
9. S. C. Clemens and W. L. Prell, *Paleoceanography* **5**, 109 (1990).
10. F. Sirocko, M. Sarnthein, H. Lange, H. Erlenkeuser, *Quat. Res.* **36**, 72 (1991).
11. F. Sirocko, thesis, University of Kiel (1995); *Palaeoecol. Afr.*, in press.
12. S. Clemens, W. Prell, D. Muray, G. Shimmield, G. Weedon, *Nature* **353**, 720 (1991).
13. G. Bond *et al.*, *ibid.* **360**, 245 (1992); B. Manighetti, I. N. McCave, M. Maslin, N. J. Shackleton, *Paleoceanography* **10**, 513 (1995).
14. E. Bard, B. Hamelin, R. G. Fairbanks, A. Zindler, *Nature* **345**, 405 (1990).
15. M. Sarnthein *et al.*, *Paleoceanography* **9**, 209 (1994).
16. S. C. Porter and A. Zisheng, *Nature* **375**, 305 (1995).
17. C. R. V. Raman and J. A. Maliekal, *ibid.* **314**, 430 (1985); T. P. Barnett, L. Dümenil, U. Schlese, E. Roeckner, M. Latif, *J. Atmos. Sci.* **46**, 661 (1989).
18. F. Gasse, V. Ledee, M. Massault, J. C. Fontes, *Nature* **342**, 57 (1989).
19. M. R. Fontugne and J. C. Duplessy, *Palaeogeogr. Palaeoclimatol. Palaeoecol.* **56**, 69 (1986); E. Van Campo, *Quat. Res.* **26**, 376 (1986).
20. D. M. Peteet, in *The Last Deglaciation: Absolute and Radiocarbon Chronologies*, E. Bard and W. S. Broecker, Eds. (NATO Advanced Study Institutes Series I, Springer-Verlag, Berlin, 1992), vol. 2., pp. 327–344.
21. W. S. Broecker, *Nature* **372**, 421 (1994).
22. J. Hansen *et al.*, in *Climate Processes and Climate Sensitivity*, J. E. Hansen and T. Takahashi, Eds. (Geophys. Monogr. 29, Maurice Ewing Vol. 5, American Geophysical Union, Washington, DC, 1984), pp. 130–163.
23. G. C. Bond and R. Lotti, *Science* **267**, 1005 (1995).
24. H. Schulz, thesis, University of Kiel (1994).
25. W. L. Prell *et al.*, *Quat. Res.* **14**, 309 (1980).
26. Using factor analysis, we can divide the 14 REEs into two factors: (i) a lithophile factor corresponding to zircon (Zr) content, which is derived from the mineral Zr abundance in Arabian dust, and (ii) a biophile factor, corresponding to lead (Pb) abundance, derived from the scavenging activity of settling biogenic detritus. The REE abundance values used in Figs. 2 through 5 are the factor scores of the lithophile factor. Substituting Zr in Figs. 2 through 5 would give the same result, but with less significance, because factor analysis removes efficiently the analytical error from the record, because all REE are extremely similar in their geochemical behavior, and only those features shared by all 14 REEs are depicted in the factor.
27. P. Pestiaux, I. van der Mersch, A. Berger, J. C. Duplessy, *Clim. Change* **12**, 9 (1988).
28. T. K. Hagelberg, G. Bond, P. deMenocal, *Paleoceanography* **9**, 545 (1994).
29. P. D. Naidu and B. A. Malmgren, *Geophys. Res. Lett.* **22**, 2361 (1995).
30. M. Stuiver, T. F. Branziunas, B. Becker, B. Kromer, *Quat. Res.* **35**, 1 (1991).
31. G. Eglinton *et al.*, *Nature* **356**, 423 (1992).
32. E. C. Grimm, G. L. Jacobson Jr., W. A. Watts, B. C. S. Hansen, K. A. Maasch, *Science* **261**, 198 (1993).
33. W. Dansgaard *et al.*, in *Climate Processes and Climate Sensitivity*, J. E. Hansen and T. Takahashi, Eds. (Geophys. Monogr. 29, Maurice Ewing Vol. 5, American Geophysical Union, Washington, DC, 1984), pp. 288–298.
34. M. Stuiver, P. M. Grootes, T. F. Braziunas, *Quat. Res.* **44**, 341 (1995).
35. A. Berger and M. F. Loutre, *Quat. Sci. Rev.* **10**, 297 (1991).
36. A. Berger, *Milankovitch Theory and Climate* (Institut d'Astronomie et de Geophysique, Universite Catholique, Louvain, Belgium, 1987).
37. J. Bloemendal and P. B. deMenocal, *Nature* **342**, 897 (1989).
38. C.-D. Garbe-Schönberg, *Geostand. Newsl.* **17**, 81 (1993).
39. D. Meese *et al.*, "Preliminary depth-age scale of the GISP2 ice core," *CRREL Spec. Rep. 94-1* (Cold Regions Research and Engineering Laboratory, Hanover, NH, 1994).
40. E. Bard, M. Arnold, R. G. Fairbanks, B. Hamelin, *Radiocarbon* **35**, (1993).

41. The ICP-MS laboratory at Kiel University was facilitated by the German Ministry of Research and Technology (grant MFG0664A); this study was funded by the Climate Research Program (grants 07KF0214 and 03F0131) from the same university. A.M. and B.M. are funded by NSF grant OCE93-13821; this is Lamont-Doherty Earth Observatory contribution 5489. The paper was begun in 1993 at the Lamont-Doherty Earth Observatory, when F.S. received a fellowship of the Max Kade Foundation, and was finished in 1995 at the Godwin Institute for Quaternary Research in Cambridge, UK, when F.S. was a fellow of the "Heisenberg" program of the German Research Council. The financial support of these institutions is gratefully acknowledged. We also thank M. Sarnthein and two anonymous reviewers for constructive comments, and S. Johnsen, J. Chappellaz, and M. Stuiver for providing ice core data. The entire data file of core 74KL (*7*, *11*) is accessible from the National Geophysical Data Center data bank, ftp.ngdc.noaa.gov, in the directory/paleo/paleocean/by_contributor/sirocko1993. For information, e-mail info@ngdc.noaa.gov

16 November 1995; accepted 7 February 1996